Journal of Nuclear Materials 535 (2020) 152178

Contents lists available at ScienceDirect

Journal of Nuclear Materials

journal homepage: www.elsevier.com/locate/jnucmat

Corrosion of uranium in liquid water under contained conditions with a headspace argon overpressure. The ternary U + $H_2O_{(l)}$ + $Ar_{(g)}$ system

A. Banos [a, *], J. Jowsey [b], A. Adamska [b], T.B. Scott [a]

[a] University of Bristol, Interface Analysis Centre, School of Physics, HH Wills Physics Laboratory, Tyndall Avenue, Bristol, BS8 1TL, United Kingdom
[b] Uranium and Reactive Metals Centre of Expertise, Sellafield Ltd, B582, Seascale, Cumbria, CA20 1PG, United Kingdom

HIGHLIGHTS

- UD_3 was identified to form in the reaction products as part of the U $D_2O_{(l)}$-Ar reaction.
- UD_3 formation confirms that hydride is produced from U and oxidation generated D_2.
- After a 'threshold' pressure (~0.5 L) is reached, UD_3 formation is facilitated.
- Ar cover gas usage in enclosed systems could lead to pressure build-up and further UH_3 formation.

ARTICLE INFO

Article history:
Received 16 January 2020
Received in revised form
10 April 2020
Accepted 14 April 2020
Available online 28 April 2020

Keywords:
Uranium
Water corrosion
Inert cover gas
Bulk-UD_3
Threshold pressure
FIB

ABSTRACT

The corrosion reaction of unirradiated uranium with deuterated liquid water under an argon (Ar) overpressure was investigated. Two samples were examined at two temperatures (55 °C and 70 °C) under an argon atmosphere and contained conditions. The rate of corrosion was derived by monitoring the pressure changes in the cell as a function of time (ascribed to D_2 generation from U-corrosion). Post-corrosion examination was conducted using FIB and XRD. Measurements of water pH were made immediately after the experiments were stopped. From the analyses, it was concluded uranium-deuteride (UD_3) was formed in the reaction products as part of the U-$D_2O_{(l)}$ -$Ar_{(g)}$ reaction. This result confirms the formation of uranium hydride/deuteride as part of the uranium-liquid water reaction in an enclosed environment, where deuteride forms through the reaction of U with oxidation-generated D_2. From reaction rate behaviour combined with post-reaction surface/interface analysis, it is suggested that after a gas 'threshold' pressure limit is reached (~0.5 bar) UD_3 formation is facilitated, leading to volume expansion and generation of stress in the overlying oxide. Breakage of this oxide would lead to direct exposure of UD_3 and U to aqueous oxidation, leading to reaction rate enhancement.

1. Introduction

In the UK, the total amount of radioactive waste is estimated at approximately 4.77 million m^3 as summarized by the Nuclear Decommissioning Authority (NDA) on April 1st, 2016 [1]. This continuous increasing stock of waste material, which requires safe handling, treatment, storage and permanent disposal, presents one of the most serious technical challenges for the nuclear industry. Intermediate level waste (ILW) represent ~6% of the total stock in the UK, the majority of which are currently interim stored in Sellafield, Cumbria, northern western of UK. ILW is mainly comprised of activated metals, contaminated metals and materials, such as reactor components, fuel-cladding and conditioned fuel parts [1]. The majority of this stock was historically kept in four legacy plants, two ponds and two silos, awaiting to be safely retrieved, transported and prepared for long-term disposal. Under wet interim storage conditions, uranium and other metals such as steel, Magnox cladding, etc. react with water to form oxides, hydroxides and hydrogen gas. For uranium, the reaction obeys Eq. (1). Due to the complex range of forms and wide variety of physical and chemical environments in which the waste is stored, hydrogen generated from oxidation of uranium and other metals may in some limited conditions become trapped, increasing in pressure in the vicinity of the metal. Indeed, events of local increase in hydrogen pressure have been documented to a higher extent in the

* Corresponding author.
E-mail addresses: antonisbanos@gmail.com, antonis.banos@bristol.ac.uk (A. Banos).

https://doi.org/10.1016/j.jnucmat.2020.152178

silos and to a lower extent in the ponds [2]. If in high concentration, H_2 may react with uranium to form UH_3 according to Eq. (2). The potential for thermal transients, thermal excursions and even pyrophoric reactions owing to the unstable nature of bulk UH_3 under sudden exposure to air and other oxidants raises serious safety and technical concerns for the industry.

$$U + 2H_2O \rightarrow UO_2 + 2H_2 \quad \text{Eq 1}$$

$$2U + 3H_2 \rightarrow 2UH_3 \quad \text{Eq 2}$$

H_2 trapping and UH_3 formation are not only possible under wet storage conditions (ponds and silos) but also after the material is retrieved from these plants. In Sellafield, after retrieval the ILW will be directed to: (a) the interim storage facility (ISF) (b) the Magnox encapsulation plant (MEP) or (c) the box encapsulation plant (BEP) where it is handled and prepared for long-term disposal [3]. Transportation of wet-corroded ILW freshly retrieved from the pond or silo plants is occurring by using metallic containers, fully sealed and in some cases under an inert gas atmosphere. This protocol is mainly followed to prevent ignition of hydrogen gas (flammable and explosive in high concentration), leading to particulate release.

In the literature, very little attention has been given to the ternary uranium-water-inert gas system. Baker et al. [4] examined the effect of hydrogen and other bystander gases such as N_2 and CO_2 on the rate and reaction products of the uranium-water system. For N_2, they used a gas overpressure up to 1013.3 mbar (1 atm) on a uranium sample corroding in liquid water, observing no effect on the kinetics of the reaction. However, on their system, the set-up was periodically opened to conduct thermogravimetric analysis. Thus, there was only a limited amount of time where the system was kept under sealed/contained conditions [5]. In previous works, the long-term corrosion reaction of uranium with liquid water in an enclosed environment have been thoroughly investigated [6–8]. The initial binary U–$H_2O_{(l)}$ and ternary U–$H_2O_{(l)}$-D_2 systems were examined. From the analysis it was found that bulk UH_3 is produced as part of the uranium-water reaction with its formation being facilitated when a critical 'threshold' hydrogen pressure is reached in the headspace volume. This 'threshold' pressure was calculated to be in the 500 mbar range, including the water vapour pressure [7]. Through the use of isotopic-labelling in the headspace environment [8], it was concluded that the hydrogen contributing to UH_3 formation is derived from the liquid water and not the headspace gas. It is considered that the free hydrogen in the headspace facilitates UH_3 formation by balancing the concentration gradient of hydrogen across the corrosion system. This finding is particularly important for this work since it was considered reasonable to go a step further and investigate if the gas threshold effect on a contained system would be observed using an inert gas in the headspace instead of hydrogen. Between nitrogen and argon, the latter is most commonly selected since uranium ignition under nitrogen is possible if the surface area of uranium is sufficiently great [9]. Argon is not reactive, however, it is important to investigate if the headspace gas could lead to decelerated rates of oxidation-generated H_2, if in quantities close to the 'threshold' pressure (~0.5 bar).

In this work, the U-$D_2O_{(l)}$-Ar system was investigated to examine the effect of an initial inert atmosphere on the kinetics and mechanism of the U + $D_2O_{(l)}$ corrosion reaction. In this way, the potential effect of the cover gas headspace pressure was evaluated, since it is a system widely used in the nuclear industry [10]. Two experiments were conducted, all using deuterated water as a reactant. The temperatures used were 55 °C and 70 °C, with Ar as the starting headspace gas for each regime. Post-examination of the reacted uranium surfaces was conducted using focused ion beam (FIB) and X-ray diffraction (XRD) analysis.

Table 1
Preliminary parameters (weight & surface area) of the samples.

Sample	Mass (g)	Surface area (cm^2)
DWAr55	4.49	3.19
DWAr70	5.69	3.84

2. Experimental

2.1. Sample provenance and preparation

Two samples were prepared for this work, all originating from the same parent batch. Extensive characterisation of the metal can be found in previous publications [6,11–13]. Table 1 integrates the initial sample parameters for the corrosion experiments. In the sample names, 'DW' indicates the liquid reactant D_2O, 'Ar' denotes the argon gas in the free volume and '55' or '70' represent the temperature of the reaction.

2.2. Reactant water

Deuterated water was used as a liquid reactant for the corrosion reaction. The water was given a three-stage freeze-vacuum-melt process to achieve anoxic reaction conditions. The gas used to fill the headspace volume for the start of each reaction was 99.99% pure Ar, provided by BOC gases.

2.3. Experimental method

A detailed description of the reaction cells and set-up used for this work can be found in Ref. [7,8]. The experimental procedure of this work was almost identical to that in Ref. [7,8] but this time argon was admitted to the volume. The mean time needed for Ar admission was approximately 2 min. To halt the reaction, the set-up was withdrawn from the oven and disconnected from the logger. The reaction pot was then immediately vented, opened and the sample carefully retrieved from the ceramic crucible containing the water. Partial mass loss of corrosion product was inevitable at this stage of the process. The sample was left in laboratory air to dry for a couple of minutes and then placed in an inert atmosphere, awaiting post-examination and analysis.

2.4. Post reaction examination

Post examination of the reacted surfaces was followed to identify the products of the corrosion reaction. A custom designed FEI FIB Strata 201 instrument was employed to physically inspect the surface and evaluate the morphological characteristics of the solid reaction products, such as UO_2. It was also used to make deep trenches in the grown corrosion layer, view the cross-section and measure its thickness. A Philips X'Pert X-ray diffractometer with a Cu-Kα source operating at 40 keV energy and 40 - 40 mA accelerating voltage allowed chemical identification of the solid corrosion products of the reactions, down to a certain depth.

2.5. Assumptions

Before proceeding to the results section, it is necessary to state and examine the validity of all the assumptions made for the analysis. For the reaction rate determination methods, it was assumed that α-U is the only solid phase in the sample, prior to reaction. Such an assumption may be regarded as broad, especially for samples with high carbon content, where carbides and carbonitrides will unavoidably be present as a trace constituent. On

such a sample, gaseous CH_4 and/or NH_3 may be evolved during corrosion [14–18]. These contributions are regarded inconsiderable since α-U is the dominant phase in the system. Additionally, the results would be comparable between the different corroding conditions since the samples have the same provenance, and all calculations were conducted using the same assumptions. The only solid and gaseous products of the U-oxidation reaction are $UO_{2(s)}$ and $D_{2(g)}$ generated as part of α-U oxidation. The exclusion of $UD_{3(s)}$ production was deliberate at this stage. For a system where hydride formation occurs, our measurements would lead to an underestimation of the corrosion rate, since oxidation-generated D_2 would not be released in the gas phase, but would react with uranium to form UD_3 (Eq. (2)). This scenario will be used later, to provide indirect evidence of hydride formation in the system based on observed changes in corrosion rate. All samples have reached the linear stage of oxide development prior to participation in the experiment. This assumption was ensured by leaving the samples exposed to air for 45 min after final preparation to ensure formation of an oxide layer sufficiently thick that a linear corrosion rate had been established. It is also assumed that no measurable reaction is taking place on the uranium surface during the time needed for water vapour saturation of the cell headspace and Ar admission to occur. A finite time period was required for every system to reach gas phase equilibrium at its set corrosion temperature. Any gas generation as part of the oxidation reaction for that time period is considered negligible and, thus, is not included in our measurements. This short period is regarded inconsiderable when compared to the total reaction time of each system (100s of hours). Moreover, it is assumed that there is negligible surface area change of the uranium sample over time with progressive corrosion. In practice, some surface area change will be observed as the sample is corroding and the metal is consumed. However, this effect will be comparable between samples. The final assumption is that negligible change in the working headspace volume of the cell occurs during progressive sample volume expansion as corrosion progresses.

3. Results

3.1. Reaction rate determination - Gas generation method

The rate of the reaction was calculated from gas pressure changes recorded in the headspace, with time. Pressure change was entirely ascribed to D_2 generation from water oxidation, relevant to Eq. (1) (D_2 is considered to behave identically to H_2). Exclusion of Eq. (2) is deliberate at this stage of the analysis since through gas generation detection: (a) it is impossible to conclude whether UH_3 is forming or not and (b) the results of this analysis will be compared with corrosion layer thickness measurements (Section 1.3.2) and could indirectly suggest whether UH_3 has formed or not. Moles of D_2 generated were converted (through Eq. (1)), to moles of reacted U per unit area with time ($mgU.cm^{-2}.h^{-1}$). Fig. 1 illustrates the corrosion progress over time for the ternary reaction systems.

3.1.1. Reaction rate line behaviour

Multiple reaction rate regimes may be observed from the graphs (Fig. 1a–b). The various reaction rate regimes, as derived from the graphs, are integrated in Table 2 (middle columns). The gas generation vs. time data from Fig. 1 were converted to mg of reacted U per unit area per hour. The mean reaction rate was derived from the: (a) differential rates derived every hour; and (b) the total U mass reaction divided by the total reaction time. The table also includes the absolute argon pressure introduced to the cell volume, at the start of the reaction.

From Fig. 1a it can be seen that sample DWAr55 exhibited two distinct reaction rate regimes, with the rate switching to higher kinetics after ~500 h of reaction. DWAr70 sample, even though having a shorter total reaction time (375 h), exhibited a more complex behaviour, with an overall of four gradients being observed through the reaction. The rate dropped considerably at ~35 h, following a two-step transition to higher kinetics at ~235 h and ~315 h, respectively.

3.1.2. Mean rate comparison to previous experiments

The mean rate values, derived from gas generation method (Table 2), were compared to previously reported rates. Baker et al. [4] examined the uranium-liquid water-nitrogen system (N_2 overpressure: 1013.3 mbar or 1 atm) and found no significant change in the corrosion rate. In that work the experimental set-up was periodically opened and, thus, the system was kept under sealed conditions for only a limited amount of time. Furthermore, that work [4] did not provide any information about the headspace volume, mass of sample or volume of water of the ternary system which, for an extended time period, could immensely affect the kinetics and products of the reaction [5]. Thus, that work was considered unsuitable for comparisons to this work. Instead, it was decided to compare the results of these experiments ($U\text{-}D_2O_{(l)}\text{-}Ar$) with those from published [6–8] and unpublished results of the uranium-water-hydrogen system, where the same experimental method was employed. The mean rate of DWAr55 sample was three to four times slower in comparison to samples reacting with water under the same regime [7] and almost twice that of a sample reacting under similar conditions but with a hydrogen overpressure. However, the mean rate was similar to that measured for the third reaction stage of the latter sample. When compared to the $U–H_2O\text{-}D_2$ system of previous works for the same temperature, the

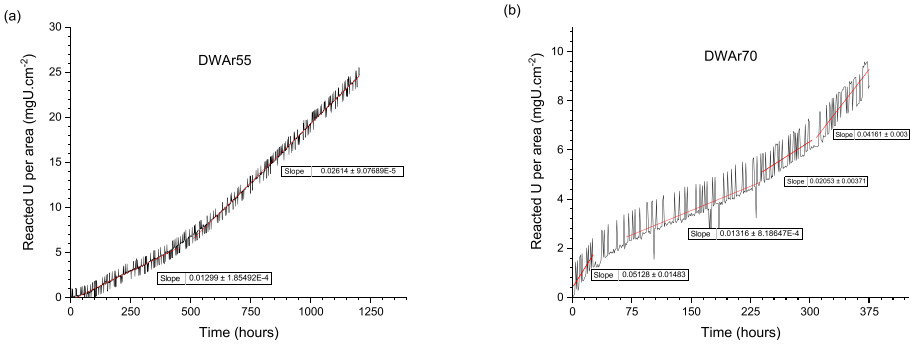

Fig. 1. Corrosion progress of uranium immersed in liquid water under an argon overpressure for: (a) DWAr55 and (b) DWAr70 sample. The rate was derived from pressure changes (ascribed to D_2 generation), converted to milligrams of reacted U per unit area, over time.

Table 2
The reaction rate regimes derived from each experimental condition, for the ternary uranium-liquid deuterated water- Argon system.

Sample	Starting headspace pressure (mbar)	Time of reaction (hours)	Headspace final pressure (Ar − D_2O − D_2) (mbar)	Reaction rate 1st regime ($mgU.cm^{-2}.h^{-1}$)	Reaction rate 2nd regime ($mgU.cm^{-2}.h^{-1}$)	Reaction rate 3rd regime ($mgU.cm^{-2}.h^{-1}$)	Reaction rate 4th regime ($mgU.cm^{-2}.h^{-1}$)	Mean reaction rate ($mgU.cm^{-2}.h^{-1}$)
DWAr55	$294.7_{(54\,^{\circ}C)}$	1203.9	676.3	n/a	n/a	0.0130 ± 0.0002	0.02610 ±0.00009	0.0206
DWAr70	$241.1_{(68.3\,^{\circ}C)}$	375	633.2	0.0513 ± 0.0148	0.0132 ±0.0008	0.0205 ±0.0037	0.042 ±0.003	0.0230

kinetics fell within the reported range (0.017–0.044 mgU cm^{-2} h^{-1} [6,8]). The DWAr70 sample was 42.5% lower in value in comparison to a sample reacting under similar conditions but with a hydrogen overpressure and a ~44% higher than that with deuterium overpressure [6,8].

3.1.3. Headspace gas overpressure effect

Deceleration of H_2 evolution owing to the pre-existing gas overpressure above a threshold value was confirmed in previous experiments [6–8]. This 'threshold pressure' was measured to be in the 450–550 mbar range [7]. For the experiments of this present work, an argon gas overpressure in the range of 200–300 mbar was initially introduced to the reaction volume to acquire a threshold pressure in the 450–550 mbar range (if P-$D_2O_{(g)}$ sat. is added) and, thus, follow the reaction until the threshold reaction stage was overtaken. Here, it must be noted that when the expression 'headspace pressure' is used, this includes oxidation-generated D_2, Ar and D_2O saturated vapour. DWAr55 started reacting with a total overpressure of ~445 mbar in the headspace. This pressure was considered sufficient for oxidation originated D_2 to decelerate in its formation in the gas phase. This could possibly justify the absence of faster kinetics at the start of the reaction. Subsequently, DWAr55 switched to faster kinetics at ~500 h and at a total pressure ~509 mbar DWAr70 exhibited a high reaction regime only during the first 35 h of reaction and at a total pressure of ~547 mbar in the headspace volume. The rate dropped considerably after that stage and remained in this slow regime for more than half of the reaction duration (~235 h). After that stage, the rate was two-step enhanced (235 h; total headspace pressure of 584 mbar) and ~315 h (607 mbar).

3.2. Reaction rate determination through oxide thickness calculation

The rate of reaction was also determined by using FIB to make a cross-section cut in the sample and to measure the thickness of the formed corroded layer. This layer was then assigned solely to UO_2 formation through Eq. (1). Such method of analysis can provide an indirect indication of whether UD_3 is forming or not. If the derived mean layer thickness, solely ascribed to UO_2 and converted to $mgU.cm^{-2}.h^{-1}$, yields a significantly higher reaction rate than that derived from the gas generation method then it is highly probable that uranium hydride is forming on the metal-oxide interface. Even though both these products, UO_2 and UH_3, have very similar density, the latter will grow in thickness without releasing any hydrogen into the gas phase (Eq. (2)). Thus, if a hydride layer is inadvertently assigned to UO_2 formation this would lead to overestimation of the rate, in comparison to the rate derived from D_2 evolution [6,8]. Additionally, UH_3, if formed, could potentially be observed but not detected through physical observation of the interface. This is due to the very robust and elliptical growth of UH_3 formation (assuming it forms with this morphology), leading to considerable volume expansion and potential destruction of the overlying oxide layer. Multiple cuts were made into each corroded surface to determine a mean thickness, recognising that variation in the thickness of the oxide may be possible.

3.2.1. Oxide morphology

Before we proceeded to comparisons between the derived rates from D_2 gas evolution and mean oxide thickness studies, the morphology of the corrosion layer was examined. Fig. 2a and b illustrate representative cross-sectional cuts into the corroded surface of each reacted sample. From physical observation of the corroded interface it can be inferred that a highly porous and brittle layer is produced on all samples. The reaction product, especially for the sample reacting at 55 °C (Fig. 2a) appears in stacked layers or sheets, separated by gaps, closely resembling UO_2 formation. In Fig. 2b, a more complex morphology may be observed, with the reaction product forming non-uniformly and expansion/strain-relief following a random direction. Since no chemical information about the corroded layer was obtained, it was not yet clear if this distinct change in morphology corresponds to uranium hydride or freshly made UO_2 of different texture.

3.2.2. Oxide thickness measurements - Reaction rate comparison

The rate-derived oxide thickness measurement was compared to that derived from gas evolution analysis. Table 3 integrates the reaction rates from both methods, along with the mean thickness of the corroded layer for each sample. In both cases, the rate derived from the thickness of the corroded layer was higher than that derived from D_2 evolution. For sample DWAr55, there was considerable loss/detachment of a flaked layer from the sample surface during retrieval and handling of the sample to prepare it for analysis. Thus, it was decided to only include thicknesses of corrosion layers which were intact in our measurements. For sample DWAr70, the oxide thickness derived rate was almost twice that obtained through gas evolution. Meso-porosity in the bulk of the oxide layer leads to overestimation of the 'real' oxide thickness even after the oxide layer 'breaks' are considered in the calculations. If meso-porosity had been included in the measurements, the differences between the rate derived from the gas evolution studies and that from oxide thickness measurements would have been smaller. Still, the consistently higher derived rates from oxide thickness determinations imply that UO_2 was not the only corrosion product produced on the metal surface. However, no direct evidence of UD_3 formation has yet been made.

3.3. XRD analysis

Fig. 3a and b display the XRD spectrum recorded for each sample. For samples DWAr70, the recorded spectra displayed only peaks associated with the oxide. Due to the substantial oxide thicknesses, the uranium peaks could not be displayed which led us to assume that the diffraction analysis did not reach the metal-oxide interface (Fig. 3b). By comparison, the sample that could be characterised down to the metal surface (DWAr55), exhibited diffraction peaks that could be assigned to U, UO_2 and UH_3 (Fig. 3a). For this sample, the recorded uranium metal and hydride peaks had

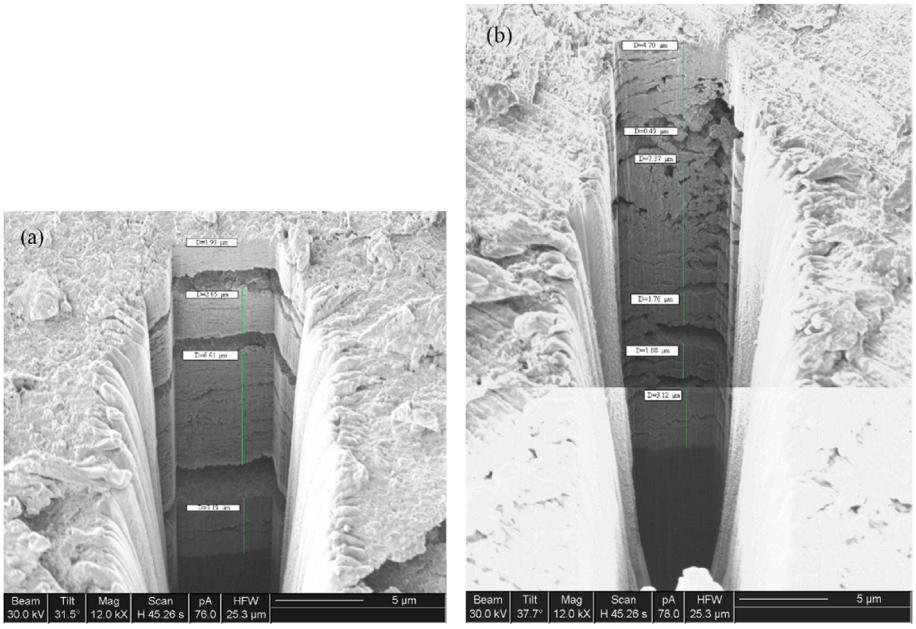

Fig. 2. Focused ion beam (FIB) milling images showing the cross-sectional view of: (a) DWAr55 and (b) DWAr70 sample. In (a) the measured thickness values represent only that part of the oxide which was adhered to the surface. A significant amount of oxide was flaked off from the surface of the DWAr55 sample. Single FIB image capture was sufficient in (a) to show the thickness of the oxide. For the other corroded sample, multiple images were produced and stitched together to demonstrate the thickness of the layer. To show the oxide in the cross-section, the periphery of the cut was inevitably saturated.

Table 3
Oxide thickness vs H_2 generation derived rate for the ternary reaction systems.

Sample	Mean oxide thickness (µm)	Reaction rate derived from mean oxide thickness measurements ($mgU.cm^{-2}.h^{-1}$)	Reaction rate derived from H_2 generation ($mgU.cm^{-2}.h^{-1}$)
DWAr55	32.74	0.0263	0.0206
DWAr70	15.88	0.041	0.0230

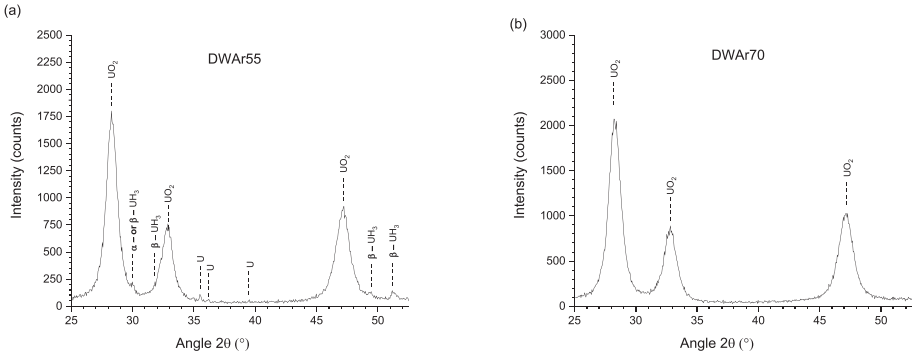

Fig. 3. Raw X-ray diffraction (XRD) spectra for: (a) DWAr55 and (b) DWAr70 samples. Analyses were performed with a Cu-K_α source, between 25 and 52.5° 2θ, 0.05° step and 5 s dwell time.

very low intensities. On this latter sample, four UD_3 peaks were identified between 25 and 52.5° (2θ) (Fig. 3a). At ~30°, the α-UD_3 and β-UD_3 phase could co-exist and overlap with each other. XRD analysis of the samples where characterisation was possible verified the existence of UD_3 on the metal-oxide interface.

4. Discussion

The long-term reaction of the U-$D_2O_{(l)}$-Ar ternary system was examined at 55 °C and 70 °C under enclosed/contained conditions. This work aimed to measure the rate of the reaction using various methods and analyse the morphology and chemical identity of the reaction products. The results of this work were compared with those of previous studies where identical experimental set-ups and conditions, but H_2 or D_2 (instead of Ar) were used in the headspace [6–8]. Argon was employed in this work to identify if the previously verified 'gas deceleration effect' is also present when an inert gas is used in the headspace. All reactions were initiated just below or at the 'threshold' headspace pressure which was previously reported to lead to reduction of H_2 gas evolution, and thus UH_3 facilitation, and found to be within the 450 - 550-mbar range [7]. From reaction rate determination through gas generation methods

(Fig. 1a and b), the reported rates were found to be similar to or slower in comparison to those for the U−$H_2O_{(l)}$-D_2 system [6,8]. In the literature, it has been reported that substitution of water with deuterated 'heavy' water leads to reduction of the oxidation kinetics [19]. If that is the case, then the results may be considered as expected. From analysing FIB cross-sectional views of the sample, measuring the thickness of the corrosion layer and fully assigning it to UO_2 through Eq. (1), the rate of the reaction could be calculated. The derived rates were found to be consistently higher than those derived from the gas generation method (Table 3). Furthermore, a very complex morphology of different texture than that of UO_2 could be observed on some of the cross-sectional faces of the samples (Fig. 2). These findings strongly imply that UO_2 is not the only phase forming in the reaction products, with uranium hydride also likely to be produced.

XRD analysis was conducted for both sample surfaces. For DWAr70, the corrosion layer was very thick, resulting in complete attenuation of the X-rays. Thus, no information about whether UD_3 or UH_3 had formed or not could be derived using XRD analysis for this sample. For sample DWAr55, peaks ascribed to UD_3 formation were detected in the spectra (Fig. 3b). This finding confirms the formation of uranium hydride as part of the uranium-liquid water reaction in an enclosed environment, where hydride forms through the reaction of U with oxidation generated H_2, and not with hydrogen originating from other sources migrating though the water to reach the U-surface and react. Of course, the latter case cannot be excluded from a real-world scenario.

By initiating the reactions with headspace gas mixture close to or at the 'threshold' pressure there was a risk of 'missing' the switch to slower kinetics of gas evolution since the 'threshold' pressure was calculated to be within the 450−550 mbar range [6,7]. However, this switch to slower gas generation kinetics was observed for one of the samples (DWAr70 − Fig. 1b). For DWAr55 which did not exhibit this behaviour (Fig. 1a), it was assumed that gas generation was effectively decelerated from the very start of the reaction (total headspace P: 445 mbar for DWAr55).

Under effective deceleration of gas generation, it is expected that UD_3 formation was facilitated. After that stage the kinetics increased rapidly. It is believed that hydride formation leads to partial breakage of the oxide over-layer, which in turn leads to: (1) oxidation of exposed UD_3 with water; and (2) enhanced oxidation kinetics of U owing to faster D_2O ingress through the ruptured/brittle oxide layer. For process 1 (UD_3 oxidation in liquid water) the rate is not linear but decelerates with time (increasing % UH_3 consumption). In the literature, a rate of 0.05−0.01 mgUH_3 consumed.mgUH_3 total^{-1}.h^{-1} is reported for a UH_3 prepared at 50 °C and reacted at 70 °C [20]. Of course, such reaction will generate 75% more D_2 gas than U-oxidation (for similar kinetics and time), according to Equations (1) and (3).

$$2UD_3 + 4D_2O \rightarrow 2UO_2 + 7D_2 \quad \text{Eq 3}$$

For DWAr55, where UD_3 formation was observed through XRD analysis, a mean rate of ~0.021 mg cm^{-2} h^{-1} was derived from the graphs at the final stage of the reaction. Such a kinetic regime falls within the expected range for the potential process of U and UD_3 oxidation.

Argon is widely used as an inert cover gas for various retrieval, transportation and storage scenarios along with helium. The main purpose of using cover gas on several storage and transportation systems is to (a) reduce corrosion in nominally dry conditions (b) Passivate potential flammable behaviour of generated H_2 building up in pressure within a container; (c) inhibit particulate release and limit interaction between the contained system and the environment. In the majority of case scenarios the pressure of argon introduced in these systems is significantly higher than the 'threshold' pressure reported above and in previous works [6,8]. In a real-world scenario where UH_3-bearing waste is kept under inert cover gas and by assuming that moisture is present within the container, based on the results above it is expected that under certain conditions, UH_3 formation may be enhanced. This is an unwanted event since, if the UH_3 manages to persist, it further enhances the possibility of a future thermal excursion. It is recognised that the use of inert cover gases is important for supressing uncontrolled thermal oxidation events for numerous different retrievals, transportation and storage scenarios. Hence, it is suggested that such a protocol (inert cover gas usage) should be utilised for the shortest time possible. A reduction in the mass of inert gas used would prove beneficial both for the safety and financial case.

5. Conclusions

The long-term reaction of the U-$D_2O_{(l)}$-Ar ternary system was examined at 55 °C and 70 °C under enclosed/contained conditions. Two samples were reacted (one for each temperature) and the rate of reaction was initially recorded using the gas generation method. Post-reaction examination of the reacted samples was performed using FIB and XRD. From the analysis, it was found that:

i. The corrosion rates derived from measured gas generation rates were comparable or slower than those reported previously for the same conditions.
ii. Uranium-deuteride was directly identified to form in the reaction products as part of the U-$D_2O_{(l)}$-Ar reaction (XRD analysis - DWAr55). This is significant since it confirms the findings of previous works [6,7] and the assumptions about the formation of uranium hydride as part of the uranium-liquid water reaction in an enclosed environment, where hydride forms through the reaction of U with oxidation-generated H_2 and not with molecular hydrogen migrating from the gas phase though the water to react at the U surface.
iii. From reaction rate behaviour combined with post-reaction surface analysis, it is suggested that after the gas threshold pressure limit is reached, UD_3 formation is facilitated. Rupture of the surface oxide by underlying hydride formation is suggested to lead to direct exposure of UD_3 and U to aqueous oxidation, leading to reaction rate enhancement (final stage of reactions - Fig. 1).

CRediT authorship contribution statement

A. Banos: Conceptualization, Methodology, Visualization, Investigation, Software, Data curation, Writing - original draft. **J. Jowsey:** Supervision, Validation, Writing - review & editing. **A. Adamska:** Conceptualization, Methodology, Visualization, Investigation. **T.B. Scott:** Supervision, Validation, Writing - review & editing.

Acknowledgements

The authors would like to thank the Engineering and Physical Sciences Research Council (EPSRC) and Sellafield Ltd for funding this project as part of 42-month PhD research studentship (Ref: 1338575), at the Interface Analysis Centre (IAC), School of Physics, University of Bristol. We would also like to thank the Sellafield Centre for Expertise in Uranium and Reactive Metals (URM) for contextual guidance and technical input.

References

[1] Nuclear Decommissioning Authority (NDA), Radioactive Wastes in the UK: A Summary of the 2016 Inventory, 2016.
[2] J. Jowsey, Sellafield Ltd, Personal Communication, 2018.
[3] Nuclear Decommissioning Authority (NDA), Radioactive waste strategy, 2018. July 2018, Doc. Ref.: ST/STY(18)0049.
[4] M.M. Baker, L. Less, S. Orman, Uranium + water reaction. Part 2. - effect of oxygen and other gases, Trans. Faraday Soc. 62 (1966) 2525–2530.
[5] M.M. Baker, L. Less, S. Orman, Uranium + water reaction. Part 1. - kinetics, products and mechanism, Trans. Faraday Soc. 62 (1966) 2513–2524.
[6] A. Banos, Investigation of Uranium Corrosion in Mixed Water - Hydrogen Environments, PhD Thesis, School of Physics, University of Bristol, 2017.
[7] A. Banos, K.R. Hallam, T. Scott, Corrosion of uranium in liquid water under vacuum contained conditions. Part 1: the initial binary U + $H_2O_{(l)}$ system, Corrosion Sci. 152 (2019) 249–260.
[8] A. Banos, K.R. Hallam, T. Scott, Corrosion of uranium in liquid water under contained conditions with a headspace deuterium overpressure. Part 2: the ternary U + $H2O_{(l)}$ + D_2 system, Corrosion Sci. 152 (2019) 261–270.
[9] W.M. Mallet, A.F. Gerds, Reaction of nitrogen with uranium, J. Electrochem. Soc. (1955) 292–296.
[10] J. Jowsey, Sellafield Ltd, Personal Communication, 2017.
[11] A. Banos, C. Jones, T. Scott, The effect of work-hardening and thermal annealing on the early stages of the uranium-hydrogen corrosion reaction, Corrosion Sci. 131 (2018) 147–155.
[12] A. Banos, T.B. Scott, Statistical analysis of UH_3 initiation using electron back-scattered diffraction (EBSD), Solid State Ionics 296 (2016) 137–145.
[13] A. Banos, C. Stitt, T. Scott, The effect of sample preparation on uranium hydriding, Corrosion Sci. 113 (2016) 91–103.
[14] R. Asuvathraman, S. Rajagopalan, K. Ananthasivan, C. Mathews, R. Mallya, Surface studies on uranium monocarbide using XPS and SIMS, J. Nucl. Mater. 224 (1995) 25–30.
[15] A. Schürenkämper, Kinetic studies of the hydrolysis of uranium monocarbide in the temperature range 30 °C –90 °C, J. Inorg. Nucl. Chem. 32 (1970) 417–429.
[16] R. Dell, V. Wheeler, N. Bridger, Hydrolysis of uranium mononitride, Trans. Faraday Soc. 63 (1967) 1286–1294.
[17] G.R. Rao, S. Mukerjee, V. Vaidya, V. Venugopal, D. Sood, Oxidation and hydrolysis kinetic studies on UN, J. Nucl. Mater. 185 (1991) 231–241.
[18] T. Scott, J. Petherbridge, N. Harker, R.J. Ball, P. Heard, J. Glascott, G. Allen, The oxidative corrosion of carbide inclusions at the surface of uranium metal during exposure to water vapour, J. Hazard Mater. 195 (2011) 115–123.
[19] H. Li, The oxidation kinetics od nitriding uranium based on ultraviolet-visible reflectance spectroscopy, Conference Paper, 48emes Journees des Actinides, Praia de Porto Novo, Portugal, 2018.
[20] D. Goddard, C. Broan, R. Orr, P. Durham, G. Woodhouse, Uranium Hydride Studies Part III: the Kinetics of Liquid Water and Water Vapour Reactions with Uranium Hydride, 12545, RP/B861/PROJ/00977/A, NNL, 2013.